Estimating spatially distributed soil water content at small watershed scales based on decomposition of temporal anomaly and time stability analysis

Wei Hu[2] and Bingcheng Si[1,2]

[1]College of Hydraulic and Architectural Engineering, Northwest A&F University, Yangling, 712100, China

[2]University of Saskatchewan, Department of Soil Science, Saskatoon, SK S7N 5A8, Canada

Correspondence to: Bingcheng Si (bing.si@usask.ca)

Abstract

Soil water content (SWC) is crucial to rainfall-runoff response at the watershed scale. A model was used to decompose the spatiotemporal SWC into a time-stable pattern (i.e, temporal mean), a space-invariant temporal anomaly, and a space-variant temporal anomaly. The space-variant temporal anomaly was further decomposed using the empirical orthogonal function (EOF) for estimating spatially distributed SWC. This model was compared to a previous model that decomposes the spatiotemporal SWC into a spatial mean and a spatial anomaly, with the latter being further decomposed using the EOF. These two models are termed temporal anomaly (TA) model and spatial anomaly (SA) model, respectively. We aimed to test the hypothesis that underlying (i.e., time-invariant) spatial patterns exist in the space-variant temporal anomaly at the small watershed scale, and to examine the advantages of the TA model over the SA model in terms of the estimation of spatially

distributed SWC. For this purpose, a dataset of near surface (0–0.2 m) and root zone (0–1.0 m) SWC, at a small watershed scale in the Canadian prairies, was analyzed. Results showed that underlying spatial patterns exist in the space-variant temporal anomaly because of the permanent controls of “static” factors such as depth to the $CaCO_3$ layer and organic carbon content. Combined with time stability analysis, the TA model improved the estimation of spatially distributed SWC over the SA model, especially for dry conditions. Further application of these two models demonstrated that the TA model outperformed the SA model at a hillslope in the Chinese Loess Plateau, but the performance of these two models in the GENCAI network (~250 km^2) in Italy was equivalent. The TA model can be used to construct a high-resolution distribution of SWC at small watershed scales from coarse-resolution remotely sensed SWC product.

Keywords: Soil moisture; Soil water downscaling; Empirical orthogonal function; Statistical models; Time stability

1. Introduction

Soil water content (SWC) of surface soils exerts a major influence on a series of hydrological processes such as runoff and infiltration (Famiglietti et al., 1998; Vereecken et al., 2007; She et al., 2013a). Soil water content in the root zone is, in many cases, linked to vegetative growth (Wang et al., 2012; Ward et al., 2012; Jia and Shao, 2013). Obtaining accurate information on the spatiotemporal SWC is crucial for improving hydrological prediction and soil water management (Venkatesh et al., 2011;

43 Champagne et al., 2012; She et al., 2013b; Zhao et al., 2013). While remote sensing
44 has advanced SWC measurements of surface soils (<5 cm in depth) at basin
45 (2,500–25,000 km^2) and continental scales (Robinson et al., 2008), characterization of
46 spatially distributed SWC at small watershed (0.1–80 km^2) scales still poses a
47 challenge. A method is needed for estimating spatially distributed SWC in the near
48 surface and root zone at watershed scales.

49 Time stability of SWC, which refers to similar spatial patterns of SWC across
50 different measurement times (Vachaud et al., 1985; Brocca et al., 2009), has been used
51 for estimating spatially distributed SWC (Starr, 2005; Perry and Niemann, 2007;
52 Blöschl et al., 2009). This method is conceptually-appealing, but assumes completely
53 time-stable spatial patterns of SWC.

54 The time-stable pattern does not explain all of the spatial variances in SWC,
55 indicating the existence of time-variant components (Starr, 2005). In order to identify
56 underlying patterns of SWC that have time-variant components, the spatiotemporal
57 SWC was decomposed into a spatial mean and a spatial anomaly. The spatial anomaly
58 of the SWC was further decomposed into the sum of the product of time-invariant
59 spatial patterns (EOFs) and temporally varying, but spatially constant coefficients
60 (ECs) using the empirical orthogonal function (EOF) (Fig. 1) (Jawson and Niemann,
61 2007; Perry and Niemann, 2007, 2008; Joshi and Mohanty, 2010; Korres et al., 2010;
62 Busch et al., 2012). Spatially distributed SWC estimates based on the decomposition
63 of spatial anomaly outperformed those based on time-stable patterns (Perry and
64 Niemann, 2007).

Recently, the spatiotemporal SWC was also decomposed into a temporal mean and a temporal anomaly (Mittelbach and Seneviratne, 2012) (Fig. 1). Previous studies indicated that the contribution of the temporal anomaly to the total spatial variance was notable (Mittelbach and Seneviratne, 2012; Brocca et al., 2014; Rötzer et al., 2015). These studies, however, only focused on surface soils at large scales (> 250 km^2). Vanderlinden et al. (2012) suggested that the temporal mean may be further decomposed into its spatial mean and residuals, and the temporal anomaly may be further decomposed into space-invariant term (i.e., spatial mean of temporal anomaly) and space-variant term (i.e., spatial residuals of temporal anomaly) (Fig. 1). Note that the spatial variance in the temporal anomaly (Mittelbach and Seneviratne, 2012) equals that of the space-variant term of the temporal anomaly (Vanderlinden et al., 2012). The further decomposition of the temporal anomaly may be physically meaningful, because the space-invariant and space-variant terms in the temporal anomaly may be forced differently. However, the models of Mittelbach and Seneviratne (2012) and Vanderlinden et al. (2012) have not been used for estimating spatially distributed SWC. If the space-variant terms are ignored during the estimation of spatially distributed SWC, their models are equivalent to that based on time-stable patterns. Therefore, estimation of spatially distributed SWC may be improved by incorporating the space-variant term of the temporal anomaly if underlying (i.e., time-invariant) spatial patterns exist in the temporal anomaly.

To our knowledge, the importance of the space-variant term of the temporal anomaly and its physical meaning at small watershed scales is not well-known. Based

87 on previous studies (Perry and Niemann, 2007; Mittelbach and Seneviratne, 2012;
88 Vanderlinden et al., 2012), we assume soil water dynamics at watershed scales can be
89 decomposed into three components (Fig. 1): (1) time-stable pattern (i.e., temporal
90 mean, spatial forcing): the "static" factors such as soil and topography control the
91 pattern; (2) space-invariant temporal anomaly (temporal forcing): the "dynamic"
92 factors such as meteorological variables and vegetation change with time, and
93 therefore modify SWC in time, regardless of spatial locations; and (3) space-variant
94 temporal anomaly (interactions between spatial forcing and temporal forcing): this
95 term represents interactions between "static" and "dynamic" factors. For example,
96 SWC recharge introduced by a rainfall may be modified by topography through
97 runoff processes; SWC loss triggered by evapotranspiration may be regulated by
98 topography through solar radiation exposure.

99 The "static" factors may be persistent in the space-variant temporal anomaly, and
100 their impacts on the space-variant temporal anomaly likely change with time. Thus,
101 we hypothesize that some underlying (i.e., time-invariant) spatial patterns exist in the
102 space-variant temporal anomaly, and their impacts can be modulated by a time
103 coefficient, both of which can be obtained by the EOF method (Fig. 1). If the
104 hypothesis is true, the estimation of spatially distributed SWC utilizing the EOF
105 decomposition may outperform the one suggested by Perry and Niemann (2007). This
106 is because: (1) the spatial anomaly which was decomposed using the EOF in Perry
107 and Niemann (2007) lumped the time-stable pattern and space-variant temporal
108 anomaly together (Fig. 1); (2) the underlying spatial patterns in the spatial anomaly

may not fully capture both time-stable patterns and patterns in the space-variant temporal anomaly due to the possible nonlinear relations between these two terms.

Therefore, the objectives were (1) to test the hypothesis that underlying spatial patterns exist in the space-variant temporal anomaly at small watershed scales and (2) to examine whether the decomposition of the space-variant temporal anomaly using the EOF has any advantages over the decomposition of the spatial anomaly (Perry and Niemann, 2007) for estimating spatially distributed SWC. Two steps were included in the estimation of spatially distributed SWC. First, the spatial mean SWC was upscaled from the SWC measurement at the most time-stable location using time stability analysis. Following this, the spatially distributed SWC was downscaled from the estimated spatial mean SWC. For the purpose of this study, spatiotemporal SWC datasets at depths of near surface (0–0.2 m) and root zone (0–1.0 m) from a Canadian prairie landscape were used. Spatiotemporal SWC of samples taken 0–0.06 m from a hillslope (100 m) in the Chinese Loess Plateau and 0–0.15 m from the GENCAI network (~250 km²) in Italy were also used to further demonstrate conditions under which the decomposition of the spatial anomaly was beneficial to the estimation of spatially distributed SWC.

2. Materials and methods

2.1 Study area and data collectionThis study was mainly conducted in the Canadian prairie pothole region (hereafter abbreviated as Canadian site) at St. Denis National Wildlife Area (52°12′ N, 106°50′ W) with an area of 3.6 km^2. This area has a humid

130 continental climate (Peel et al., 2007), and had a mean annual air temperature of
131 1.9 °C and a mean annual precipitation of 402 mm during the study period (Fig. 2). A
132 variety of depressions, knolls, and knobs result in a sequence of undulating slopes
133 (Biswas et al., 2011). The elevation varies from 554.8 to 557.5 m. The soils are
134 dominated by clay loam textured Mollisols (Soil Survey Staff, 2010) and covered by
135 mixed grass, i.e., smooth brome grass (*Bromus inermis*) and alfalfa (*Medicago sativa*
136 L.). The near surface soil porosity ranges from 38% (knolls) to 70% (depressions).
137 Calcium carbonates ($CaCO_3$) derived mostly from fragments of limestone rocks are
138 common in the Canadian Prairies. The $CaCO_3$ is dissolved by the slightly acidic
139 rainwater moving through the upper horizons and deposited to lower horizons. The
140 heterogeneous amount of infiltrated water resulted in a varying depth of $CaCO_3$ layer
141 ranging from almost 0 m in the knolls to 2.1 m in the depressions. A 576 m long
142 sampling transect with 128 sampling locations spaced at 4.5 m intervals was
143 established over several rounded knolls and depressions. At each location, a time
144 domain reflectometry probe was used to measure SWC of the near surface soil (0–0.2
145 m), and a neutron probe was used to collect SWC measurements at 0.2 m intervals
146 between a depth of 0.2 and 1.0 m. The SWC was measured on a volumetric basis and
147 expressed as a percentage (%) volume of water per unit soil volume. The SWC of the
148 root zone was calculated by averaging the SWC of 0–0.2, 0.2–0.4, 0.4–0.6, 0.6–0.8,
149 and 0.8–1.0 m. Soil water content was measured on 23 dates from July 17, 2007 to
150 September 29, 2011. The SWC dataset was collected in all seasons except winter, and
151 accurately portrays the variations in soil water conditions in the study area. In addition

to the SWC dataset, the soil, vegetative, and topographical properties were obtained at each sampling location. These properties included soil particle components (clay, silt, and sand contents), bulk density, soil organic carbon (SOC) content for the surface layer, A horizon depth, C horizon depth, depth to the $CaCO_3$ layer, leaf area index, elevation, cos(aspect), slope, curvature, gradient, upslope length, solar radiation, specific contributing area, convergence index, wetness index, and flow connectivity. Detailed information on the measurements can be found in Biswas et al. (2012). The datasets from the Canadian site were used to demonstrate the following two aspects in detail: (1) different components of spatiotemporal SWC and their contributing factors, and (2) the advantages of the new decomposition method over the method suggested by Perry and Niemann (2007) in terms of the estimation of spatially distributed SWC.

Besides the Canadian site, datasets from a hillslope scale in a Chinese site and a large watershed scale in a Italian site were applied. Along a hillslope of 100 m in length in the Chinese Loess Plateau, SWC of 0–0.06 m was measured 136 times from June 25, 2007 to August 30, 2008 by a Delta-T Devices Theta probe (ML2x) at 51 locations (Hu et al., 2011). The hillslope was covered by *Stipa bungeana* Trin. and *Medicago sativa* L. in sandy loam and silt loam soils. In the GENCAI network (~250 km^2) in Italy, SWC of 0–0.15 m was measured by a TDR probe at 46 locations, 34 times from February to December in 2009 (Brocca et al., 2012, 2013). The GENCAI area was dominated by grassland with a flat topography, in silty clay soils. With these two datasets, spatially distributed SWC was estimated using the two different decomposition methods. Performances in estimation of spatially distributed SWC

were compared among all three sites to further demonstrate conditions under which the new decomposition outperformed the method suggested by Perry and Niemann (2007).

2.2 Statistical models for decomposing soil water content

Spatiotemporal SWC at small watershed scales was decomposed into three components: time-stable pattern, space-invariant temporal anomaly, and space-variant temporal anomaly. This model was compared to the one that decomposed SWC into spatial mean and spatial anomaly (Perry and Niemann, 2007). Both the space-variant temporal anomaly and spatial anomaly were decomposed using the EOF method. The two models are termed temporal anomaly (TA) model and spatial anomaly (SA) model, respectively. Figure 1 displays the differences between the two models. Each component will be explained in detail later. The explanation of nomenclatures is listed in Table A1. Because we focus on estimating spatial distribution of SWC at any given time, only spatial variances of SWC were taken into account. Therefore, the variance or covariance denotes the quantity in space without specifications.

2.2.1 The SA model

Perry and Niemann (2007) expressed SWC at location n and time t (S_{tn}) as (Fig. 1):

$$S_{tn} = S_{t\hat{n}} + Z_{tn}, \qquad (1)$$

where $S_{t\hat{n}}$ is the spatial mean SWC at time t (temporal forcing) and Z_{tn} is the spatial anomaly of SWC (lumped spatial forcing and interactions). The subscript $\hat{n}$ ($\hat{t}$) indicates a space (time) averaged quantity.

According to Perry and Niemann (2007), $S_{t\hat{n}}$ can be estimated by remote sensing,

197 water balance models, and in situ soil water measurement at a representative (or
198 time-stable) location. The in situ soil water measurement method was selected
199 because the representative location can be easily determined with prior SWC datasets.
200 By measuring SWC only at the most time-stable location (*s*) and future time *t* (S_{ts}),
201 $S_{t\hat{n}}$ can be estimated using (Grayson and Western, 1998):

202 $$S_{t\hat{n}} = \frac{S_{ts}}{1+\delta_{\hat{ts}}} \quad , \qquad (2)$$

203 where the *s* was identified using the time stability index of mean absolute bias error
204 (Hu et al., 2010, 2012). The $\delta_{\hat{ts}}$ is the temporal mean relative difference of SWC at
205 the *s*, which was calculated with prior measurements.

206 Spatial anomaly (Z_{tn}) can be reconstructed by the sum of the product of
207 time-invariant spatial structures (EOFs) and temporally varying coefficients (ECs)
208 using the EOF method (Perry and Niemann, 2007; Joshi and Mohanty, 2010;
209 Vanderlinden et al., 2012). The ECs correspond to the eigenvectors of the matrix of
210 spatial covariance of the Z_{tn}, and the EOFs are obtained by projecting the Z_{tn} onto
211 the matrix ECs as: $\mathrm{EOFs} = Z_{tn}\,\mathrm{EC}s$. The number of EOF (or EC) series equals the
212 number of sampling dates. Each EOF series corresponds to one value at each location,
213 and each EC series has one value at each measurement time. Each EOF is chosen to
214 be orthogonal to other EOFs, and the lower-order EOFs account for as much variance
215 as possible. The sum of variances of all EOFs equals the sum of variances of Z_{tn}
216 from all measurement times.

217 Usually, a substantial amount of variance can be explained by a small number of
218 EOFs. Johnson and Wichern (2002) suggested the eigenvalue confidence limits

method for selecting the number of EOFs. Once the number of significant EOFs at a confidence level of 95% is selected, Z_{tn} can be estimated as the sum of the product of significant EOFs and associated ECs as:

$$Z_{tn} = \sum \mathrm{EOF}^{sig} \times (\mathrm{EC}^{sig})^{T}, \quad (3)$$

where EOF^{sig} represents the significant EOFs of the Z_{tn} obtained during model development, EC^{sig} is the associated temporally varying coefficient, and the superscript *T* represents matrix transpose. Following Perry and Niemann (2007), the associated significant EC at time *t* (EC_t), is estimated by the cosine relationship between EC and $S_{t\hat{n}}$ developed using prior measurements:

$$\mathrm{EC}_t = a + b\cos\left(\frac{2\pi}{c} S_{t\hat{n}} - d\right), \quad (4)$$

where *a*, *b*, *c*, and *d* are the fitted parameters using prior measurements and $S_{t\hat{n}}$ is estimated from Eq. (2). By using the continuous function, EC_t can be estimated at any $S_{t\hat{n}}$ values, which allows for the estimation of spatially distributed SWC at any soil water conditions.

2.2.2 The TA model

Mittelbach and Seneviratne (2012) decomposed the S_{tn} into a time-stable pattern (i.e., temporal mean) and a temporal anomaly component (Fig. 1):

$$S_{tn} = M_{\hat{t}n} + A_{tn}, \quad (5)$$

where $M_{\hat{t}n}$ is the time-stable pattern (spatial forcing) controlled by "static" factors such as soil properties and topography; A_{tn} refers to the temporal anomaly (lumped temporal forcing and interactions). The variance of SWC ($\sigma^2_{\hat{n}}(S_{tn})$) is the sum of variance of the $M_{\hat{t}n}$ ($\sigma^2_{\hat{n}}(M_{\hat{t}n})$), variance of the A_{tn} ($\sigma^2_{\hat{n}}(A_{tn})$), and two times of

241 covariance between $M_{\hat{t}n}$ and A_{tn} ($2\mathrm{cov}(M_{\hat{t}n}, A_{tn})$), which can be expressed as:

242 $$\sigma^2_{\hat{n}}\left(S_{tn}\right) = \sigma^2_{\hat{n}}\left(M_{\hat{t}n}\right) + 2\,\mathrm{cov}(M_{\hat{t}n}, A_{tn}) + \sigma^2_{\hat{n}}\left(A_{tn}\right). \quad (6)$$

243 Because the A_{tn} in Mittelbach and Seneviratne (2012) is a lumped term, it can be
244 further decomposed into space-invariant temporal anomaly ($A_{t\hat{n}}$, i.e., temporal
245 forcing) and space-variant temporal anomaly (R_{tn}, i.e., interactions) (Vanderlinden et
246 al., 2012). At a watershed scale, the $A_{t\hat{n}}$ is controlled by temporally varying factors
247 such as meteorological variables and vegetation. Positive and negative $A_{t\hat{n}}$
248 correspond to relatively wet and dry periods, respectively. The R_{tn} refers to the
249 redistribution of $A_{t\hat{n}}$ among different locations due to the interactions between
250 spatial forcing and temporal forcing. For example, soil and topography regulate how
251 much rainfall enters soil and how much water runs off or runs on at a location. This,
252 in turn, dictates vegetation growth in a water-limited environment. Therefore, S_{tn}
253 can also be expressed as (Fig. 1):

254 $$S_{tn} = M_{\hat{t}n} + A_{t\hat{n}} + R_{tn}. \quad (7)$$

255 The temporal trends of $A_{t\hat{n}}$ in Eq. (7) and $S_{t\hat{n}}$ in Eq. (1) are the same as both
256 represent temporal forcing. Because the $A_{t\hat{n}}$ is space-invariant and orthogonal to the
257 $M_{\hat{t}n}$ and R_{tn} in a space, $\sigma^2_{\hat{n}}\left(S_{tn}\right)$ in Eq. (6) can also be written as:

258 $$\sigma^2_{\hat{n}}\left(S_{tn}\right) = \sigma^2_{\hat{n}}\left(M_{\hat{t}n}\right) + 2\,\mathrm{cov}(M_{\hat{t}n}, R_{tn}) + \sigma^2_{\hat{n}}\left(R_{tn}\right), \quad (8)$$

259 where $\mathrm{cov}(M_{\hat{t}n}, R_{tn})$ is the covariance between the $M_{\hat{t}n}$ and R_{tn}, and $\sigma^2_{\hat{n}}\left(R_{tn}\right)$ is
260 the variance of the R_{tn}. Apparently, $2\,\mathrm{cov}(M_{\hat{t}n}, R_{tn})$ equals $2\,\mathrm{cov}(M_{\hat{t}n}, A_{tn})$, and
261 $\sigma^2_{\hat{n}}\left(R_{tn}\right)$ equals $\sigma^2_{\hat{n}}\left(A_{tn}\right)$. The percent (%) of $\sigma^2_{\hat{n}}\left(M_{\hat{t}n}\right)$, $2\,\mathrm{cov}(M_{\hat{t}n}, R_{tn})$, and
262 $\sigma^2_{\hat{n}}\left(R_{tn}\right)$ out of the $\sigma^2_{\hat{n}}\left(S_{tn}\right)$ are calculated. The $\mathrm{cov}(M_{\hat{t}n}, R_{tn})$ can be negative at

some conditions, for example, when the depressions correspond to greater $M_{\hat{t}n}$ and more negative R_{tn} values in the discharge periods. This resulted in percentage of $\sigma^2_{\hat{n}}(M_{\hat{t}n})$ and $\sigma^2_{\hat{n}}(R_{tn})$ > 100% and percentage of $2\mathrm{cov}(M_{\hat{t}n}, R_{tn})$ < 0% (Mittelbach and Seneviratne, 2012; Brocca et al., 2014; Rötzer et al., 2015). If R_{tn} is zero at any time or location, there are no interactions between spatial forcing and temporal forcing, $\sigma^2_{\hat{n}}(S_{tn})$ and the spatial trends of SWC are consistent over time. Therefore, R_{tn} is directly responsible for temporal change in the spatial variability of SWC.

If some underlying spatial patterns exist in R_{tn}, R_{tn} can be reconstructed by the sum of the product of time-invariant spatial structures (EOFs) and time-dependent coefficients (ECs) using the EOF method. Note that the number of EOF (or EC) series also equals the number of sampling dates.

For estimation of spatially distributed SWC, R_{tn} is estimated by the same method as Z_{tn} using Eq. (3). The $M_{\hat{t}n}$ is estimated with prior measurements by:

$$M_{\hat{t}n} = \frac{1}{m}\sum_{j=1}^{m} S_{tn}, \qquad (9)$$

where m is the number of previous measurement times, and $A_{t\hat{n}}$ is estimated by:

$$A_{t\hat{n}} = S_{t\hat{n}} - M_{\hat{t}\hat{n}}, \qquad (10)$$

where $M_{\hat{t}\hat{n}}$ is the spatial mean of $M_{\hat{t}n}$, and $S_{t\hat{n}}$ is estimated from SWC measurements at the most time-stable location using Eq. (2).

The Pearson correlation coefficient (R) is used to explore the linear relationships between various spatial components in the two models (i.e., EOF1 of the Z_{tn} in the SA model, $M_{\hat{t}n}$, and EOF1 of the R_{tn} in the TA model) and environmental factors

285 (i.e., soil, vegetative, and topographical properties). The multiple stepwise regressions
286 are conducted to determine the percentage of variations in the spatial components
287 which the controlling factors explain.

288 **2.3 Validation and performance parameter**

289 The TA model is more complicated than the SA model. In order to evaluate the two
290 models for parsimony, AICc values are calculated (Burnham and Anderson, 2002) as:

291 $$\mathrm{AICc} = 2k + n\ln(RSS/n) + 2k(k+1)/(n-k-1), \qquad (11)$$

292 where k is the number of parameters, n is the sample size, and RSS is the residual sum
293 of squares.

294 Both cross validation and split sample validation are used to estimate SWC
295 distribution with both models. For the cross validation, an iterative removal of 1 of the
296 23 dates is made for model development, and the SWC along the transect
297 corresponding to the removed date is estimated iteratively. For the split sample
298 validation, SWC from 14 dates of the first two years (from July 17, 2007 to May 27,
299 2009) is used for model development, and the SWC distribution of 9 dates in the
300 second two years (from July 21, 2009 to September 29, 2011) is estimated.

301 The Nash-Sutcliffe coefficient of efficiency (NSCE) is used to evaluate the quality
302 of estimation of spatially distributed SWC, which is expressed as:

303 $$\mathrm{NSCE} = 1 - \frac{\sigma_{\varepsilon}^2}{\sigma_{measure}^2}, \qquad (12)$$

304 where $\sigma_{measure}^2$ is the variance of measured SWC, and σ_{ε}^2 is the mean squared
305 estimation error. A larger NSCE value implies a better quality of estimation. A paired
306 samples T-test is used to test whether the NSCE values between the TA model and the

SA model are statistically significant at $P<0.05$.

Many factors may affect the relative performance of spatially distributed SWC estimation between the TA model and the SA model. First, the degree of outperformance of the TA model over the SA model may depend on the amount of R_{tn} variance considered in the TA model. On one hand, the two models are identical if variance of R_{tn} is close to zero or there are negligible interactions between the spatial and temporal components (Fig. 1). On the other hand, if no underlying spatial patterns exist in the R_{tn} or the underlying spatial patterns accounted for little variance of the R_{tn}, the outperformance will also be very limited. Therefore, the greater the variance of R_{tn} considered in the TA model, the more likely the TA model can outperform the SA model. Second, the way of EOF decomposition may also affect the relative performance. In the SA model, EOF decomposition is performed on lumped time-stable patterns ($M_{\hat{t}n}$) and space-variant temporal anomaly (R_{tn}). In the TA model, however, EOF decomposition is made only on the R_{tn}. In theory, the two models will be identical if the $M_{\hat{t}n}$ and the first underlying spatial pattern (i.e., EOF1) of the R_{tn} were perfectly correlated. If a nonlinear relationship exists between them, lumping the $M_{\hat{t}n}$ and R_{tn} together, as in the SA model, would weaken the model performance as compared to the TA model. From this aspect, the greater deviation from a linear relationship between the $M_{\hat{t}n}$ and EOF1 of the R_{tn}, may lead to a greater outperformance of the TA model over the SA model. Finally, the performances of both models rely on the estimation accuracy of the EC_t which depends on both goodness of fit of the cosine function (i.e., Eq. 4) and

329 estimation accuracy of the $S_{t\hat{n}}$. Because the same $S_{t\hat{n}}$ values are used for the two
330 models, the relative performance of the two models is related to the goodness of fit of
331 Eq. (4).

332 # 3. Results

333 ## 3.1 Components of SWC and their controls

334 ### 3.1.1 Spatial mean ($S_{t\hat{n}}$) and spatial anomaly (Z_{tn})

335 The values of spatial mean ($S_{t\hat{n}}$) in the SA model varied with the seasons (Fig. 3a).
336 In the spring, such as May 2, 2008 and April 20, 2009, snowmelt infiltration resulted
337 in relatively great $S_{t\hat{n}}$ values. In the summer, however, even one month after large
338 rainfall events (such as on July 19, 2008 and June 21, 2009), the high
339 evapotranspiration by fast-growing vegetation resulted in small $S_{t\hat{n}}$ values. The
340 values of $S_{t\hat{n}}$ also varied between inter-annual meteorological conditions. In 2008,
341 there was less precipitation and higher air temperature than in 2010 (Fig. 2). As a
342 result, $S_{t\hat{n}}$ was relatively smaller in 2008 than in 2010.

343 The spatial patterns of spatial anomaly (Z_{tn}) were similar to those of the original
344 SWC patterns (Fig. 3a). The values of Z_{tn} in wet periods (e.g., May 13, 2011) were
345 much greater than in dry periods (e.g., August 23, 2008) in depressions (e.g., at a
346 distance of 123 and 250 m); at other locations, however, the spatial anomaly was
347 slightly less in wet periods than in dry periods for both soil layers. Moreover, the
348 spatial anomaly in depressions during the wet periods was much greater in the near
349 surface than in the root zone.

When SWCs of all 23 dates were used for model development, only EOF1 was statistically significant (Fig. 4a), which accounted for 84.3% (0–0.2 m) and 86.5% (0–1.0 m) of the variances in the Z_{tn}. Correlation analysis indicated that the spatial pattern of EOF1 in the Z_{tn} was identical to the time-stable patterns ($M_{\hat{t}n}$) in the TA model (R=1.0). The controls of EOF1 was therefore the same as those of $M_{\hat{t}n}$, and will be discussed later. The relationship between associated EC1 and $S_{t\hat{n}}$ can be fitted well by the cosine function (R^2=0.73 at both the near surface and root zone) (Fig. 4b).

3.1.2 Time-stable pattern ($M_{\hat{t}n}$), space-invariant temporal anomaly ($A_{t\hat{n}}$), and space-variant temporal anomaly (R_{tn})

Figure 3b displays the three components in the TA model. The first component $M_{\hat{t}n}$ fluctuated along the transect, with high values in depressions and low values on knolls; the $M_{\hat{t}n}$ also had greater spatial variability in the near surface (variance =36.7%^{2}) than in the root zone (variance=19.5%^{2}). For both soil layers, SOC, depth to the $CaCO_3$ layer, sand content, and wetness index are the dominant factors of $M_{\hat{t}n}$; they together explained 74.5% (near surface) and 75.6% (root zone) of the variances in the $M_{\hat{t}n}$ (Table 1). In addition, the temporal trend of $A_{t\hat{n}}$ was the same as that of $S_{t\hat{n}}$ in the SA model (Fig. 3a) as both represent temporal forcing.

The R_{tn} varied among landscape positions (Fig. 3b). At a sampling distance of 123 m (in a depression), R_{tn} was negative in dry periods such as August 23, 2008 and positive in wet periods such as May 13, 2011. This was true for all depressions for both the near surface and the root zone. Therefore, topographically lower positions

usually corresponded to more positive R_{tn} during the wet periods and more negative R_{tn} during the dry periods. Furthermore, the absolute values of R_{tn} were generally greater in the near surface than the root zone, indicating a greater space-variant temporal anomaly for shallower depths.

The SWC variances and associated components (Eq. 8) also varied with time (Fig. 5). Often, wetter conditions corresponded to greater $\sigma^2_{\hat{n}}(S_{tn})$, as further indicated by moderate correlation between $\sigma^2_{\hat{n}}(S_{tn})$ and $S_{t\hat{n}}$ (R^2 of 0.51 and 0.38 for the near surface and the root zone, respectively). This was in agreement with others (Gómez-Plaza et al., 2001; Martínez-Fernández and Ceballos, 2003; Hu et al., 2011). Furthermore, there were greater $\sigma^2_{\hat{n}}(S_{tn})$ values at near surface than in the root zone, indicating greater variability of SWC in the near surface.

The time-invariant $\sigma^2_{\hat{n}}(M_{\hat{t}n})$ accounted for the $\sigma^2_{\hat{n}}(S_{tn})$ with percentages ranging from 25 to 795% for the near surface and from 40 to 174% for the root zone (Fig. 5). The $\sigma^2_{\hat{n}}(M_{\hat{t}n})$ exceeded the $\sigma^2_{\hat{n}}(S_{tn})$ mainly under dry conditions, such as July–October in 2008 and 2009. This excess was offset by the $\sigma^2_{\hat{n}}(R_{tn})$ and $2\mathrm{cov}(M_{\hat{t}n}, R_{tn})$, with the latter accounting for the $\sigma^2_{\hat{n}}(S_{tn})$ negatively with mean absolute percentages of 210% for the near surface and 17% for the root zone. In the dry period, the absolute percentage of $2\mathrm{cov}(M_{\hat{t}n}, R_{tn})$ was up to 1327% for the near surface and 122% for the root zone. These values are comparable to those in Mittelbach and Seneviratne (2012) and Brocca et al. (2014).

The $\sigma^2_{\hat{n}}(R_{tn})$ accounted for less percentage of the $\sigma^2_{\hat{n}}(S_{tn})$ than other

components did (Fig. 5). The percentages of $\sigma_{\hat{n}}^2(R_{tn})$ ranged from 11 to 632% (arithmetic average of 118%) for the near surface and from 6 to 48% (arithmetic average of 19%) for the root zone; the percentage of $\sigma_{\hat{n}}^2(R_{tn})$ tended to be greater in drier periods. This indicates that the space-variant temporal anomaly cannot be ignored, particularly in dry conditions. Furthermore, the percentage of $\sigma_{\hat{n}}^2(R_{tn})$ was greater in the near surface than in the root zone, confirming stronger temporal dynamics of soil water at the near surface. Compared with larger scale studies (Mittelbach and Seneviratne, 2012; Brocca et al., 2014), the percentage of $\sigma_{\hat{n}}^2(R_{tn})$ out of the $\sigma_{\hat{n}}^2(S_{tn})$ at the near surface was greater, with a mean percentage of 118%, versus 9–68% in the other, larger scale studies. This indicates that interactions between spatial and temporal forcing were stronger, resulting in relatively more intensive temporal dynamics of soil water in our study area than at larger scales.

Three significant EOFs of R_{tn} for both soil layers were identified when SWC of all 23 dates were used for model development. The first three EOFs explained 61.1, 13.4, and 8.1% respectively, of the total R_{tn} variance for the near surface, and 44.3, 20.2, and 12.4%, respectively, of the total R_{tn} variance in the root zone. Therefore, our hypothesis that underlying spatial patterns exist in the R_{tn} was supported. Due to the negligible contribution of EOF2 and EOF3 to the estimation of spatially distributed SWC, only EOF1 is shown in Fig. 6a. The associated EC1 changed with soil water conditions ($S_{t\hat{n}}$) (Fig. 6b). When SWC was close to average levels, the EC1 was close to 0, resulting in negligible R_{tn}. This was in accordance with Mittelbach and Seneviratne (2012) and Brocca et al. (2014), who showed that the spatial variance

of the temporal anomaly was the smallest when water contents were close to average levels. The cosine function (Eq. 4) explained a large amount of the variances in EC1 for both soil layers (R^2=0.76 at the near surface and 0.88 in the root zone).

The contribution of EOF1 to the space-variant temporal anomaly can be examined through the product of the EOF1 and the associated EC1. The EC1 values tended to be positive during wet periods and negative during dry periods (Fig. 6b); more positive EOF1 values were usually observed at locations with greater $M_{\hat{tn}}$ values (Figs. 3b and 6a). Therefore, the product of EOF1 and EC1 led to greater temporal SWC dynamics at wetter locations of both layers in both the wet and dry periods.

Depth to the $CaCO_3$ layer and SOC had significant, positive correlations with EOF1 for both soil layers (R ranging from 0.76 to 0.88; Table 1). They jointly accounted for 81.6% (near surface) and 81.0% (root zone) of the variances in EOF1. This implies that locations with a greater depth to the $CaCO_3$ layer and SOC, which correspond to wetter locations such as depressions, usually have greater temporal SWC dynamics during both wet and dry periods.

3.2 Estimation of spatially distributed SWC

When all 23 datasets were used and only EOF1 was considered, the TA model had an AICc value of 4093 for the near surface and 562 for the root zone, while the corresponding values for the SA model were 6370 and 3460. This indicated that even when penalty to complexity was given, the TA model was better than the SA model. The two models in terms of spatially distributed SWC estimation are compared below.

3.2.1 The TA model

437 The R_{tn} terms and associated EOFs differed slightly with each validation. The
438 number of significant EOFs varied between one (accounting for 60% of the total cases)
439 and three for both soil layers. A paired samples T-test indicated that more EOFs did
440 not result in a significant increase of NSCE in the estimation of spatially distributed
441 SWC for both validation methods. This is also supported by the increasing AICc
442 values with the increasing number of parameters resulting from more EOFs (data not
443 shown). This indicates that higher-order EOFs, even if they are statistically significant,
444 are negligible for SWC prediction. Therefore, SWC distribution was estimated with
445 EOF1 only.

446 Estimated SWCs generally approximated those measured at different soil water
447 conditions during the cross validation (Fig. 7). However, on October 27, 2009, there
448 were unsatisfactory overestimates at the 100–140 and 220–225 m locations near the
449 surface (Fig. 7a). Unsatisfactory NSCE values of -4.05, -1.83, and -3.81 were
450 obtained in the near surface in only three of the 23 dates, which were all in the fall
451 (October 22, 2008, August 27, 2009, and October 27, 2009, respectively). The poor
452 performance obtained with the TA model on those dates (Fig. 8a) was a result of
453 overestimation in depressions, which is shown for example on October 27, 2009 (Fig.
454 7a). These dates also corresponded to a high percentage of $\sigma_{\hat{n}}^2(R_{tn})$ to the $\sigma_{\hat{n}}^2(S_{tn})$
455 (203–439%). For August 23 and September 17 in 2008, which were in dry periods,
456 the percentage of $\sigma_{\hat{n}}^2(R_{tn})$ at the near surface was also high (580 and 630%).
457 Because a fair amount of $\sigma_{\hat{n}}^2(R_{tn})$ was accounted for with the TA model, the TA
458 model performed satisfactorily (NSCE of 0.43 and 0.60). For the remaining 20 dates,

459 the resulting NSCE value ranged from 0.38 to 0.90 in the near surface and from 0.65
460 to 0.96 in the root zone (Fig. 8). This suggests that the TA model was generally
461 satisfactory, with better performance in the root zone than in the near surface.

462 During the split sample validation, the TA model resulted in SWC estimations with
463 NSCE values ranging from 0.61 to 0.85 near the surface and from 0.32 to 0.92 in the
464 root zone, with exception of two days (August 27, 2009 and October 27, 2009 with
465 NSCE values of -2.63 and -5.12, respectively) at 0–0.2 m (Fig. 8). This suggested that
466 the TA model performed well in estimating spatially distributed SWC patterns except
467 on August 27, 2009 and October 27, 2009 at 0–0.2 m. The estimation in the root zone
468 was also generally better than in the near surface.

469 **3.2.2 Comparison with the SA model**

470 One significant EOF of Z_{tn} was identified for both soil layers, irrespective of the
471 validation method. The SA model with only EOF1 produced reasonable SWC
472 estimations for both validations in all dates in the root zone and in every date except
473 five dates (August 23, 2008, September 17, 2008, October 22, 2008, August 27, 2009,
474 and October 27, 2009) in the near surface (Fig. 8). Similarly, when more EOFs were
475 included, NSCE values did not increase significantly (data not shown) and
476 consequently, estimation of spatially distributed SWC was not improved. This was
477 because EOF2 and EOF3 together explained a very limited (<10%) amount of
478 variability of Z_{tn} and thus had low predictive power in terms of variance.

479 The difference in NSCE values between the TA and SA models for both validations
480 are presented in Fig. 9. Generally, the difference decreased as $A_{t\hat{n}}$ increased, and

then slightly increased with a further increase in $A_{t\hat{n}}$. A paired samples T-test indicated that the NSCE values of the TA model were significantly (P<0.05) greater than those of the SA model for both soil layers, irrespective of validation methods. This indicates that the TA model outperformed the SA model, particularly in dry conditions. This was because when the soil was dry, there was a high percentage of $\sigma^2_{\hat{n}}(R_{tn})$, and thus strong variability in the space-variant temporal anomaly.

3.3 Further application at other two sites with different scales

3.3.1 A hillslope in the Chinese Loess Plateau

On average, the $\sigma^2_{\hat{n}}(M_{\hat{t}n})$, $\sigma^2_{\hat{n}}(R_{tn})$, and $2\mathrm{cov}(M_{\hat{t}n}, R_{tn})$ accounted for 53, 74 and -27% out of the $\sigma^2_{\hat{n}}(S_{tn})$, indicating that both time-stable pattern and temporal anomalies were the main contributors to the $\sigma^2_{\hat{n}}(S_{tn})$. The EOF analysis showed that only the EOF1 was statistically significant for both the R_{tn} and Z_{tn}, and the EOF1 explained 23% and 47% of the total variances of R_{tn} and Z_{tn}, respectively. This illustrated that underlying spatial patterns exist in the R_{tn} on the hillslope. Cross validation was used to estimate the spatially distributed SWC along the hillslope. The results showed that the NSCE varied from -4.25 to 0.83 (TA model) and from -4.30 to 0.81 (SA model), with a mean value of 0.25 and 0.19, respectively (Fig. 10a). A paired samples T-test showed that the NSCE values for the TA model were significantly (P<0.05) greater than those for the SA model, indicating that the TA model outperformed the SA model. As Fig. 10a shows, the outperformance was greater when SWC deviated from intermediate conditions, especially for dry conditions, which was similar to the Canadian site.

3.3.2 The GENCAI network in Italy

The $\sigma^2_{\hat{n}}(M_{\hat{t}n})$, $\sigma^2_{\hat{n}}(R_{tn})$, and $2\mathrm{cov}(M_{\hat{t}n}, R_{tn})$ accounted for 38, 68, and -7% out of the $\sigma^2_{\hat{n}}(S_{tn})$ (Brocca et al., 2014), indicating the dominant role of temporal anomalies in SWC variability. The first three EOFs of the R_{tn} explained 19, 16, and 8% of the total $\sigma^2_{\hat{n}}(R_{tn})$, and no EOFs were statistically significant, indicating that no underlying spatial patterns exist in the R_{tn}. The EOF1 of the Z_{tn} was significant and accounted for 37% of the variances in the Z_{tn}. Although the EOF1 of the R_{tn} was not significant, it was considered in the TA model for estimating spatially distributed SWC. The cross validation indicates that the NSCE varied from -0.79 to 0.50 (TA model) and from -0.87 to 0.56 (SA model), with mean values of 0.09 and 0.08, respectively (Fig. 10b). The SWC estimation based on these two models was not satisfactory except for a few days. As Fig. 10b shows, the differences in NSCE values between the two models were scattered around 0. A paired samples T-test showed that the NSCE values between the TA model and the SA model were not significant (P<0.05), indicating no differences in estimating spatially distributed SWC between these two models.

4 Discussion

4.1 Controls of the $M_{\hat{t}n}$ and R_{tn}

The R_{tn} played an important role in the temporal change in spatial patterns of the SWC. The underlying spatial patterns and physical meaning in the R_{tn} were examined in our study for the first time. Although three significant EOFs of the R_{tn}

524 existed in some cases, only EOF1 rather than higher-order EOFs of the R_{tn} should
525 be considered for the spatially distributed SWC estimation. Among many factors
526 influencing the EOF1 of the R_{tn}, depth to the $CaCO_3$ layer followed by the SOC,
527 were the most important factors. Depressions have deeper $CaCO_3$ layers than knolls,
528 and the shallow $CaCO_3$ layer on knolls limited water infiltration during rainfall or
529 snowmelt, resulting in less water recharge on knolls than in depressions. The depth to
530 $CaCO_3$ layer and SOC were negatively correlated with elevation (R=-0.54, P<0.01).
531 Therefore, the influence of depth to $CaCO_3$ layer and SOC partially reflected the role
532 of topography in driving snowmelt runoff along slopes in the spring, which
533 contributes to increasing water recharge in depressions. As already demonstrated,
534 topographically lower positions corresponded to more negative R_{tn} during the dry
535 periods. This implies that depressions lost more water during discharge. This is
536 because depressions usually corresponded to vegetation with a larger leaf area index,
537 which would result in higher evapotranspiration and more water loss during discharge
538 periods.

539 As Table 1 shows, both the depth to the $CaCO_3$ layer and SOC controlled the $M_{\hat{t}n}$.
540 This was because deeper $CaCO_3$ layers and higher SOC were observed in depressions
541 where soils were usually wetter in most of the year because of the snowmelt runoff in
542 the spring and rainfall runoff in the summer and autumn (van der Kamp et al., 2003).
543 Therefore, the roles of soil and topography were two-fold: On one hand, they were
544 highly correlated with the time-stable patterns and thus the time stability of SWC
545 (Gómez-Plaza et al., 2000; Mohanty and Skaggs, 2001; Grant et al., 2004); On the

other hand, soil and topography, interplaying with temporal forcing, triggered local-specific soil water change and destroyed time stability of SWC. Their roles in protecting time stability persisted, but their roles in destroying time stability varied with time. Greater $\sigma_{\hat{n}}^2(R_{tn})$ implies greater contribution of these factors in soil water dynamics, resulting in less time stability of SWC.

4.2 Model performance for spatially distributed SWC estimation

The outperformance of the TA model for estimating spatial SWC at the Canadian site and Chinese site can be partly explained by the high percentages (average of 19–118%) of the $\sigma_{\hat{n}}^2(R_{tn})$ out of the total variance. When SWC is close to average levels, R_{tn} is also close to zero, resulting in negligible percentage of $\sigma_{\hat{n}}^2(R_{tn})$. In this case, the soil water patterns are stable in time, the SA model performs well, and there will be little differences between these two models. As is well known, the spatial patterns in soil water content are inherently time unstable. For example, when evapotranspiration becomes the dominant process at the small watershed scale, more water will be lost in depressions due to the denser vegetation than on knolls (Millar, 1971; Biswas et al., 2012), effectively diminishing the spatial patterns and increasing temporal instability. In this case, the $\sigma_{\hat{n}}^2(R_{tn})$ accounts for more percentage of the total variance (e.g., high up to 632%) and the TA model may outperform the SA model. This explained why the outperformance of the TA model was more obvious in the dry conditions. For the GENCAI network in Italy, although the $\sigma_{\hat{n}}^2(R_{tn})$ accounted for 68% of the total variance, the performance of the TA model was identical to the SA model. This was because there were no underlying spatial patterns

568 in the R_{tn}. Similarly, because the first underlying spatial pattern (i.e., EOF1)
569 explained greater percentages of the $\sigma_{\hat{n}}^2(R_{tn})$ at the Canadian site (44–61%) than the
570 Chinese site (23%), the outperformance of the TA model over the SA model was more
571 obvious at the former site (Fig. 9 and 10a). Therefore, the TA model is advantageous
572 only if the percentage of $\sigma_{\hat{n}}^2(R_{tn})$ out of the total variance is substantial and
573 underlying spatial patterns exist in the R_{tn}.

574 The existence of underlying spatial patterns in the R_{tn} is related to the controlling
575 factors, which may be scale-specific. At small scales, "static" factors such as the depth
576 to the $CaCO_3$ layer and SOC at the Canadian site may affect not only the time-stable
577 patterns but also the R_{tn}. The persistent influence of "static" factors on the R_{tn}
578 resulted in significant underlying spatial patterns in the R_{tn}. Thus, the TA model
579 outperformed the SA model at the small scales. At large scales such as the basin scale
580 or greater, time-stable patterns may be controlled by, in addition to soil and
581 topography (Mittelbach and Seneviratne, 2012), the climate gradient (Sherratt and
582 Wheater, 1984); at those scales, R_{tn} is more likely to be controlled by the
583 meteorological anomaly (i.e., spatially random variation) (Walsh and Mostek, 1980),
584 and the effects of soil and topography may be reduced. Consequently, spatial patterns
585 in the R_{tn} may be weakened and the TA model may have no advantages over the SA
586 model such as for the Italian site.

587 The $M_{\hat{tn}}$ and the underlying spatial patterns (EOF1) in the R_{tn} were controlled
588 by the same spatial forcing (e.g., depth to $CaCO_3$ layer and SOC) at the Canadian site
589 (Table 1), and they were correlated with an R^2 of 0.83 for the near surface and 0.42 for

590 the root zone. Although the relationships between $M_{\hat{t}n}$ and R_{tn} were strong, they
591 were not strictly linear, suggesting that $M_{\hat{t}n}$ and R_{tn} were affected differently by
592 these factors. Therefore, the nonlinear relationship between $M_{\hat{t}n}$ and R_{tn} partially
593 contributed to the outperformance of the TA model over the SA model.

594 The relationship between the $S_{t\hat{n}}$ and EC1 was better fitted by the cosine function
595 in the TA model than the SA model (Figs. 4b and 6b), with R^2 of 0.76 versus 0.73 in
596 the near surface and 0.88 versus 0.73 in the root zone. The reduced scatter in the $S_{t\hat{n}}$
597 and EC1 relationship for the TA model may also partly explain the outperformance of
598 the TA model over the SA model.

599 Therefore, the outperformance of the TA model over the SA model depends on
600 counterbalance among the variance of R_{tn} explained in the TA model, the linear
601 correlation between the $M_{\hat{t}n}$ and EOF1 of the R_{tn}, and the goodness of fit for the
602 $S_{t\hat{n}}$ and EC1 relationship. For example, the variance of EOF1 in the R_{tn} for the
603 near surface (i.e., $264\%^2$) was much greater than that for the root zone (i.e., $43\%^2$).
604 However, $M_{\hat{t}n}$ and underlying spatial patterns (EOF1) in the R_{tn} in the root zone
605 deviated more from a linear relationship, and the reduced scatter in the $S_{t\hat{n}}$ and EC1
606 relationship in the TA model was more obviously in the root zone than in the near
607 surface. As a result, the outperformance of the TA model was comparable between the
608 near surface and root zone at the Canadian site (Fig. 9).

609 In the real world, the relations between the $M_{\hat{t}n}$ and underlying spatial patterns in
610 the R_{tn} may rarely be perfectly linear. Therefore, when underlying spatial patterns
611 exist in the R_{tn} and the R_{tn} has substantial variances, the TA model is preferable

to the SA model for the estimation of spatially distributed SWC. On the contrary, when underlying spatial patterns does not exist in the R_{tn} or the R_{tn} has negligible variances, the SA model may be selected although these two models yield the same quality of SWC estimation. This is because the TA model needs one more spatial parameter (i.e., $M_{\hat{tn}}$) than the SA model.

Previous studies on SWC decomposition mainly focus on near surface layers (Jawson and Niemann, 2007; Perry and Niemann, 2007, 2008; Joshi and Mohanty, 2010; Korres et al., 2010; Busch et al., 2012). This study decomposed spatiotemporal SWC using the TA model for both the near surface and the root zone. The results showed that the estimation of spatially distributed SWC at small watershed scales was improved by the TA method that considers the R_{tn}. The $\sigma^2_{\hat{n}}\left(M_{\hat{tn}}\right)$ was greater than the $\sigma^2_{\hat{n}}\left(R_{tn}\right)$ (Fig. 5), indicating that time stability was more important than time instability for SWC estimation. For the three dates in the fall (i.e., October 22, 2008, August 27, 2009, and October 27, 2009), strong evapotranspiration and deep drainage in depressions resulted in a much lower SWC at the near surface than in the spring. This resulted in reduced time stability of SWC pattern and poor performance of both models and validation methods in terms of SWC evaluation (Fig. 8a). Because of the stronger time stability of SWC in deeper soil layers (Biswas and Si, 2011), SWC evaluation was more accurate for soil layers extending from the surface to greater depth. This is particularly important because SWC data for deeper soil layers in a watershed is more difficult to collect than that of surface soil.

5 Conclusions

The TA model was used to decompose spatiotemporal SWC into time-stable patterns $M_{\hat{t}n}$, space-invariant temporal anomaly $A_{t\hat{n}}$, and space-variant temporal anomaly R_{tn}. This study indicated that underlying spatial patterns may exist in the R_{tn} at small scales (e.g., small watersheds and hillslope) but may not exist at large scales such as the GENCAI network (~250 km²) in Italy. This was because the R_{tn} at small scales was driven by "static" factors such as depth to the $CaCO_3$ layer and SOC at the Canadian site, while the R_{tn} at large scales may be dominated by "dynamic" factors such as meteorological anomaly. Compared to the SA model, estimation of spatially distributed SWC was improved with the TA model at small watershed scales. This was because the TA model considered a fair amount of spatial variance in the R_{tn}, which was ignored in the SA model. Furthermore, the improved performance was observed mainly when there was less or more soil water than the average level, especially in drier conditions due to the high $\sigma_{\hat{n}}^2(R_{tn})$ value.

This study showed that outperformance of the TA model over the SA model is possible when $\sigma_{\hat{n}}^2(R_{tn})$ accounts for substantial variance of SWC, and significant spatial patterns (or EOFs) exist in the R_{tn}. Further application of the TA model for the estimation of spatially distributed SWC at different scales and hydrological backgrounds is recommended. If the TA model parameters (i.e., $M_{\hat{t}n}$, EOF1 of the R_{tn}, and relationship between EC and $S_{t\hat{n}}$) are obtained from historical in-situ SWC datasets, a detailed spatially distributed SWC of near surface soil at watershed scales can be constructed from remotely sensed SWC. Note that both models rely on

in-situ SWC measurements for model parameters. Therefore, future research should be conducted to estimate spatially distributed SWC in un-gauged watersheds based on the estimation of the model parameters using pedotransfer functions. The codes for decomposing SWC with the SA and TA models and related EOF analysis were written in Matlab and are freely available from the authors upon request.

Acknowledgements

This project was funded by the National Science Foundation of China (K305021308) and the Natural Sciences and Engineering Research Council (NSERC) of Canada. We thank Dr. Asim Biswas, Dr. Henry Wai Chau, Mr. Trent Pernitsky, and Mr. Eric Neil for their help in data collection. We thank the anonymous reviewers and the Editor for their constructive comments.

References

Biswas, A., Chau, H. W., Bedard-Haughn, A., and Si, B. C.: Factors controlling soil water storage in the Hummocky landscape of the Prairie Pothole region of North America, Can. J. Soil Sci., 92, 649–663, doi: 10.4141/CJSS2011-045, 2012.

Biswas, A. and Si, B. C.: Scales and locations of time stability of soil water storage in a hummocky landscape, J. Hydrol., 408, 100–112, doi: 10.1016/j.jhydrol.2011.07.027, 2011.

Blöschl, G., Komma, J., and Hasenauer, S.: Hydrological downscaling of soil moisture, Final report to the H-SAF (Hydrology Satellite Application Facility) via the

675 Austrian Central Institute for Meteorology and Geodynamics (ZAMG), Vienna
676 University of Technology, A-1040 Vienna, Austria, 2009.
677 Brocca, L., Melone, F., Moramarco, T., and Morbidelli, R.: Soil moisture temporal
678 stability over experimental areas in Central Italy, Geoderma, 148, 364–374, doi:
679 10.1016/j.geoderma.2008.11.004, 2009.
680 Brocca, L., Tullo, T., Melone, F., Moramarco, T., and Morbidelli, R.: Catchment scale
681 soil moisture spatial-temporal variability, J. Hydrol., 422-423, 63–75,
682 doi:10.1016/j.jhydrol.2011.12.039, 2012.
683 Brocca, L., Zucco, G., Mittelbach, H., Moramarco, T., and Seneviratne, S. I.: Absolute
684 versus temporal anomaly and percent of saturation soil moisture spatial variability for
685 six networks worldwide, Water Resour. Res., 50, 5560–5576, doi:
686 10.1002/2014WR015684, 2014.
687 Brocca, L., Zucco, G., Moramarco, T., and Morbidelli, R.: Developing and testing a
688 long-term soil moisture dataset at the catchment scale, J. Hydrol., 490, 144–151, doi:
689 10.1016/j.jhydrol.2013.03.029, 2013.
690 Burnham, K. P. and Anderson, D. R.: Model selection and multimodel inference: A
691 practical information-theoretic approach (2nd ed.), Springer-Verlag, New York, 2002.
692 Busch, F. A., Niemann, J. D., and Coleman, M.: Evaluation of an empirical
693 orthogonal function-based method to downscale soil moisture patterns based on
694 topographical attributes, Hydrol. Process., 26, 2696–2709, doi: 10.1002/hyp.8363,
695 2012.
696 Champagne, C., Berg, A. A., McNairn, H., Drewitt, G., and Huffman, T.: Evaluation

of soil moisture extremes for agricultural productivity in the Canadian prairies, Agric. For. Meteorol., 165, 1–11, doi: 10.1016/j.agrformet.2012.06.003, 2012.

Famiglietti, J. S., Rudnicki, J. W., and Rodell, M.: Variability in surface moisture content along a hillslope transect: Rattlesnake Hill, Texas, J. Hydrol., 210, 259–281, doi: 10.1016/S0022-1694(98)00187-5, 1998.

Gómez-Plaza, A., Alvarez-Rogel, J., Albaladejo, J., and Castillo, V. M.: Spatial patterns and temporal stability of soil moisture across a range of scales in a semi-arid environment, Hydrol. Process., 14, 1261–1277, doi: 10.1002/(SICI)1099-1085(200005)14:7<1261::AID-HYP40>3.0.CO;2-D, 2000.

Gómez-Plaza, A., Martínez-Mena, M., Albaladejo, J., and Castillo, V. M.: Factors regulating spatial distribution of soil water content in small semiarid catchments, J. Hydrol., 253, 211–226, doi: 10.1016/S0022-1694(01)00483-8, 2001.

Grant, L., Seyfried, M., and McNamara, J.: Spatial variation and temporal stability of soil water in a snow-dominated, mountain catchment, Hydrol. Process., 18, 3493–3511, doi: 10.1002/hyp.5789, 2004.

Grayson, R. B. and Western, A. W.: Towards areal estimation of soil water content from point measurements: Time and space stability of mean response, J. Hydrol., 207, 68–82, doi: 10.1016/S0022-1694(98)00096-1, 1998.

Hu, W., Shao, M. A., Han, F. P., and Reichardt, K.: Spatio-temporal variability behavior of land surface soil water content in shrub- and grass-land, Geoderma, 162, 260–272, doi: 10.1016/j.geoderma.2011.02.008, 2011.

Hu, W., Shao, M. A., and Reichardt, K.: Using a new criterion to identify sites for

719 mean soil water storage evaluation, Soil Sci. Soc. Am. J., 74, 762–773, doi:
720 10.2136/sssaj2009.0235, 2010.
721 Hu, W., Tallon, L. K., and Si, B. C.: Evaluation of time stability indices for soil water
722 storage upscaling, J. Hydrol., 475, 229–241, doi: 10.1016/j.jhydrol.2012.09.050,
723 2012.
724 Jawson, S. D. and Niemann, J. D.: Spatial patterns from EOF analysis of soil moisture
725 at a large scale and their dependence on soil, land-use, and topographic properties,
726 Adv. Water Resour., 30, 366–381, doi:10.1016/j.advwatres.2006.05.006, 2007.
727 Jia, Y. H. and Shao, M. A.: Temporal stability of soil water storage under four types of
728 revegetation on the northern Loess Plateau of China, Agric. Water Manage., 117,
729 33–42, doi: 10.1016/j.agwat.2012.10.013, 2013.
730 Johnson, R. A. and Wichern, D. W.: Applied multivariate statistical analysis, Prentice
731 Hall, Upper Saddle River, New Jersey, 2002.
732 Joshi, C. and Mohanty, B. P.: Physical controls of near-surface soil moisture across
733 varying spatial scales in an agricultural landscape during SMEX02, Water Resour.
734 Res., 46, doi: 10.1029/2010WR009152, 2010.
735 Korres, W., Koyama, C. N., Fiener, P., and Schneider, K.: Analysis of surface soil
736 moisture patterns in agricultural landscapes using Empirical Orthogonal Functions,
737 Hydrol. Earth Syst. Sci., 14, 751–764, doi: 10.5194/hess-14-751-2010, 2010.
738 Martínez-Fernández, J. and Ceballos, A.: Temporal stability of soil moisture in a
739 large-field experiment in Spain, Soil Sci. Soc. Am. J., 67, 1647–1656, 2003.
740 Millar, J. B.: Shoreline-area ratios as a factor in rate of water loss from small sloughs,

741 J. Hydrol., 14, 259–284, doi: 10.1016/0022-1694(71)90038-2, 1971.
742 Mittelbach, H. and Seneviratne, I.: A new perspective on the spatio-temporal
743 variability of soil moisture: Temporal dynamics versus time-invariant contributions,
744 Hydrol. Earth Syst. Sci., 16, 2169–2179, doi: 10.5194/hess-16-2169-2012, 2012.
745 Mohanty, B. P. and Skaggs, T. H.: Spatio-temporal evolution and time–stable
746 characteristics of soil moisture within remote sensing footprints with varying soil
747 slope and vegetation, Adv. Water Resour., 24, 1051–1067, doi:
748 10.1016/S0309-1708(01)00034-3, 2001.
749 Peel, M. C., Finlayson, B. L., and McMahon, T. A.: Updated world map of the
750 Köppen-Geiger climate classification, Hydrol. Earth Syst. Sci., 11, 1633–1644,
751 doi:10.5194/hess-11-1633-2007, 2007.
752 Perry, M. A. and Niemann J. D.: Analysis and estimation of soil moisture at the
753 catchment scale using EOFs, J. Hydrol., 334, 388–404, doi:
754 10.1016/j.jhydrol.2006.10.014, 2007.
755 Perry, M. A. and Niemann J. D.: Generation of soil moisture patterns at the catchment
756 scale by EOF interpolation, Hydrol. Earth Syst. Sci., 12, 39–53,
757 doi:10.5194/hess-12-39-2008, 2008.
758 Robinson, D. A., Campbell, C. S., Hopmans, J. W., Hornbuckle, B. K., Jones, S. B.,
759 Knight, R., Ogden, F., Selker, J., and Wendroth, O.: Soil moisture measurement for
760 ecological and hydrological watershed-scale observatories: A review, Vadose Zone J.,
761 7, 358–389, doi: 10.2136/vzj2007.0143, 2008.
762 Rötzer, K., Montzka, C., and Vereecken, H.: Spatio-temporal variability of global soil

763 moisture products, J. Hydrol., 522, 187–202, doi: 10.1016/j.jhydrol.2014.12.038,
764 2015.
765 She, D. L., Liu, D. D., Peng, S. Z., and Shao, M. A.: Multiscale influences of soil
766 properties on soil water content distribution in a watershed on the Chinese Loess
767 Plateau, Soil Sci., 178, 530–539, doi: 10.1016/j.jhydrol.2014.08.034, 2013a.
768 She, D. L., Xia, Y. Q., Shao, M. A., Peng, S. Z., and Yu, S. E.: Transpiration and
769 canopy conductance of Caragana Korshinskii trees in response to soil moisture in
770 sand land of China, Agrofor. Syst., 87, 667–678, doi: 10.1007/s10457-012-9587-4,
771 2013b.
772 Sherratt, D. J. and Wheater, H. S.: The use of surface-resistance soil-moisture
773 relationships in soil-water budget models, Agric. For. Meteorol., 31, 143–157, doi:
774 10.1016/0168-1923(84)90016-9, 1984.
775 Soil Survey Staff: Soil Taxonomy, 11th edition, USDA National Resources
776 Conservation Services, Washington DC, 2010.
777 Starr, G. C.: Assessing temporal stability and spatial variability of soil water patterns
778 with implications for precision water management, Agric. Water Manage., 72,
779 223–243, doi: 10.1016/j.agwat.2004.09.020, 2005.
780 Vachaud, G., De Silans, A. P., Balabanis, P., and Vauclin, M.: Temporal stability of
781 spatially measured soil water probability density function, Soil Sci. Soc. Am. J., 49,
782 822–828, 1985.
783 van der Kamp, G., Hayashi, M., and Gallen, D.: Comparing the hydrology of grassed
784 and cultivated catchments in the semi-arid Canadian prairies, Hydrol. Process., 17,

559–575, doi: 10.1002/hyp.1157, 2003.

Vanderlinden, K., Vereecken, H., Hardelauf, H., Herbst, M., Martinez, G., Cosh, M. H., and Pachepsky, Y. A.: Temporal stability of soil water contents: A review of data and analyses, Vadose Zone J., 11, 4, doi: 10.2136/vzj2011.0178, 2012.

Vereecken, H., Kamai, T., Harter, T., Kasteel, R., Hopmans, J., and Vanderborght, J.: Explaining soil moisture variability as a function of mean soil moisture: A stochastic unsaturated flow perspective, Geophys. Res. Lett., 34, L22402, doi: 10.1029/2007GL031813, 2007.

Venkatesh, B., Nandagiri, L., Purandara, B. K., and Reddy, V. B.: Modelling soil moisture under different land covers in a sub-humid environment of Western Ghats, India, J. Earth Syst. Sci., 120, 387–398, 2011.

Walsh, J. E. and Mostek, A.: A quantitative-analysis of meteorological anomaly patterns over the United-States, 1900–1977, Mon. Weather Rev., 108, 615–630, doi: 10.1175/1520-0493(1980)108<0615:AQAOMA>2.0.CO;2, 1980.

Wang, Y. Q., Shao, M. A., Liu. Z. P., and Warrington, D. N.: Regional spatial pattern of deep soil water content and its influencing factors, Hydrolog. Sci. J., 57, 265–281, doi: 10.1080/02626667.2011.644243, 2012.

Ward, P. R., Flower, K. C., Cordingley, N., Weeks, C., and Micin, S. F.: Soil water balance with cover crops and conservation agriculture in a Mediterranean climate, Field Crop. Res., 132, 33–39, doi: 10.1016/j.fcr.2011.10.017, 2012.

Zhao, Y., Peth, S., Wang, X. Y., Lin, H., and Horn, R.: Controls of surface soil moisture spatial patterns and their temporal stability in a semi-arid steppe, Hydrol.

807 Process., 24, 2507–2519, doi: 10.1002/hyp.7665, 2010.

Figure captions

Figure 1. Decomposition of spatiotemporal soil water content (SWC) in different models.

Figure 2. Daily mean air temperature and precipitation during the study period.

Figure 3. Components of soil water content in (a) the SA model (spatial mean soil water content $S_{t\hat{n}}$ and spatial anomaly Z_{tn}) and in (b) the TA model (time-stable pattern $M_{\hat{t}n}$, space-invariant temporal anomaly $A_{t\hat{n}}$, and space-variant temporal anomaly R_{tn}) for 0–0.2 and 0–1.0 m. Also shown is the elevation.

Figure 4. (a) The EOF1 of the spatial anomaly Z_{tn} and (b) relationships of associated EC1 versus spatial mean soil water content Z_{tn} fitted by the cosine function (Eq. 4).

Figure 5. Spatial variances of different components in Eq. (8) expressed in $\%^2$ (upper panel) and as percentage (lower panel) for (a) 0–0.2 and (b) 0–1.0 m. Spatial mean soil water content $S_{t\hat{n}}$ on each measurement day is also shown.

Figure 6. (a) The EOF1 of the space-variant temporal anomaly R_{tn} and (b) relationships of associated EC1 versus spatial mean soil water content $S_{t\hat{n}}$ fitted by the cosine function (Eq. 4).

Figure 7. Estimated soil water content (SWC) versus measured SWC for three dates at different soil water conditions (August 23, 2008, October 27, 2009, and May 13, 2011 are associated with relatively dry, medium, and wet days, respectively) using the TA model for (a) 0–0.2 and (b) 0–1.0 m.

Figure 8. The Nash-Sutcliffe coefficient of efficiency (NSCE) of soil water content

estimation using the TA and SA models for (a) 0–0.2 and (b) 0–1.0 m for both cross validation (CV) and split sample validation (SV). At 0–0.2 m, three dates (October 22, 2008, August 27, 2009, and October 27, 2009) as indicated by green lines present negative NSCE values (-4.05, -1.83, and -3.81, respectively, for the CV on the three dates; -2.63 and -5.12, respectively, for the SV on the latter two dates). Spatial mean soil water content $S_{t\hat{n}}$ on each measurement day is also shown.

Figure 9. Nash-Sutcliffe coefficient of efficiency (NSCE) difference between the TA and SA models in terms of soil water content estimation using both cross validation (CV) and split sample validation (SV) as a function of space-invariant temporal anomaly $A_{t\hat{n}}$ for (a) 0–0.2 and (b) 0–1.0 m.

Figure 10. Nash-Sutcliffe coefficient of efficiency (NSCE) difference between the TA and SA models in terms of soil water content estimation using cross validation as a function of space-invariant temporal anomaly $A_{t\hat{n}}$ for (a) 0–0.06 m of the Chinese Loess Plateau hillslope and (b) 0–0.15 m of the GENCAI network in Italy. The NSCE values for both models are also shown.

Table 1. Pearson correlation coefficients between time-stable pattern $M_{\hat{t}n}$, EOF1 of space-variant temporal anomaly R_{tn} and various properties.

	0–0.2 m		0–1.0 m	
	$M_{\hat{t}n}$	EOF1	$M_{\hat{t}n}$	EOF1
Sand content	-0.52**	-0.36**	-0.66**	-0.26**
Silt content	0.29**	0.14	0.40**	0.06
Clay content	0.43**	0.38**	0.51**	0.33**
Organic carbon	0.78**	0.83**	0.73**	0.76**
Wetness index	0.64**	0.59**	0.68**	0.56**
Depth to $CaCO_3$ layer	0.77**	0.84**	0.65**	0.88**
A horizon depth	0.51**	0.62**	0.44**	0.65**
C horizon depth	0.66**	0.69**	0.58**	0.76**
Bulk density	-0.58**	-0.67**	-0.46**	-0.62**
Elevation	-0.24**	-0.28**	-0.24**	-0.32**
Specific contributing area	0.20*	0.24**	0.24**	0.23**
Convergence index	-0.58**	-0.56**	-0.55**	-0.58**
Curvature	-0.10	-0.08	-0.19*	-0.16
Cos(aspect)	0.05	0.04	0.08	0.05
Gradient	-0.12	-0.09	-0.21*	-0.02
Slope	-0.51**	-0.48**	-0.56**	-0.44**
Upslope length	0.19*	0.21*	0.21*	0.25**
Solar radiation	-0.07	0.03	-0.11	0.08
Flow connectivity	0.45**	0.43**	0.49**	0.49**
Leaf area index	-0.07	0.06	-0.10	-0.14
Variance explained[1]	74.5%	81.6%	75.6%	81.0%

[1]percent of variance explained by the controlling factors obtained by the multiple stepwise regressions.
*Significant at $P<0.05$; ** Significant at $P<0.01$.

Table A1. Notations.

$M_{\hat{t}\hat{n}}$	spatial mean of $M_{\hat{t}n}$
R_{tn}	space-variant temporal anomaly of SWC at location *n* and time *t*
$A_{t\hat{n}}$	space-invariant temporal anomaly of SWC at time *t*
Z_{tn}	spatial anomaly of SWC at location *n* and time *t*
$S_{t\hat{n}}$	spatial mean SWC at time *t*
$\sigma^2_{\hat{n}}$	spatial variance
A_{tn}	temporal anomaly of SWC at location *n* and time *t*
$\delta_{\hat{t}n}$	temporal mean relative difference of SWC at location *n*
COV	spatial covariance
S_{tn}	SWC at location *n* and time *t*
$M_{\hat{t}n}$	time-stable pattern of SWC
ECs	temporally-varying coefficients of R_{tn} (or Z_{tn})
EOFs	time-invariant spatial structures of R_{tn} (or Z_{tn})
NSCE	Nash-Sutcliffe coefficient of efficiency
R	Pearson correlation coefficient
SWC	soil water content

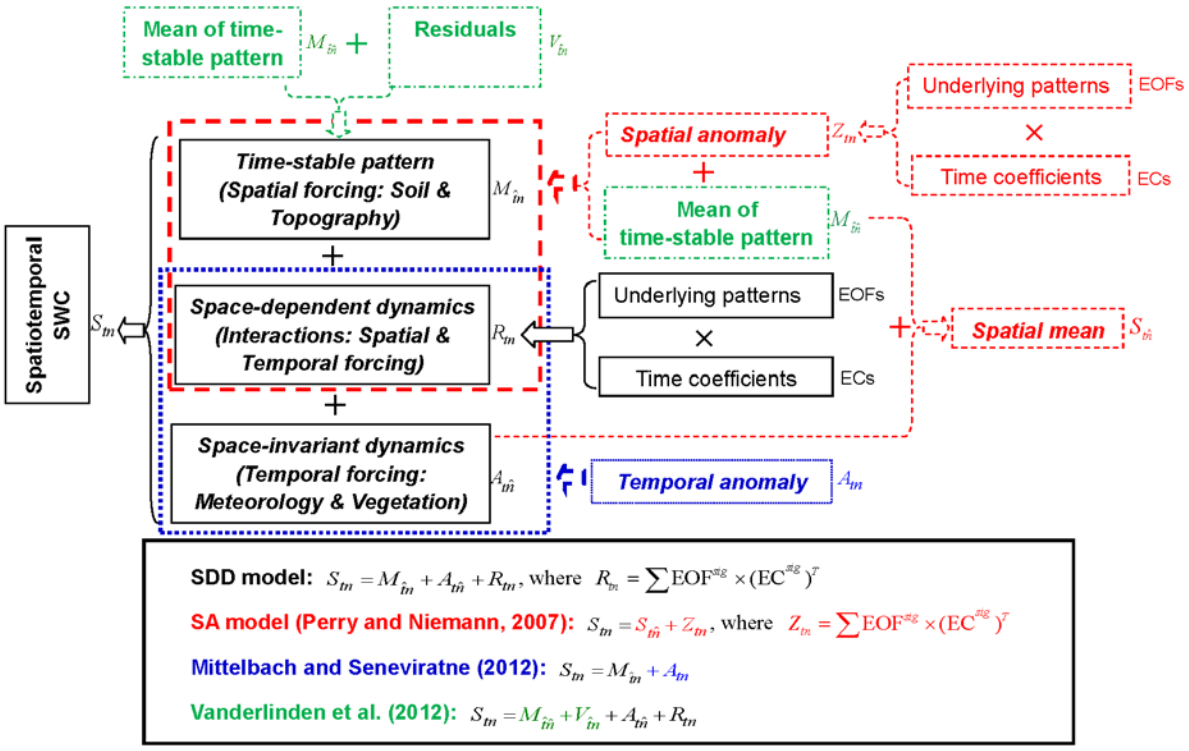

Fig. 1. Decomposition of spatiotemporal soil water content (SWC) in different models.

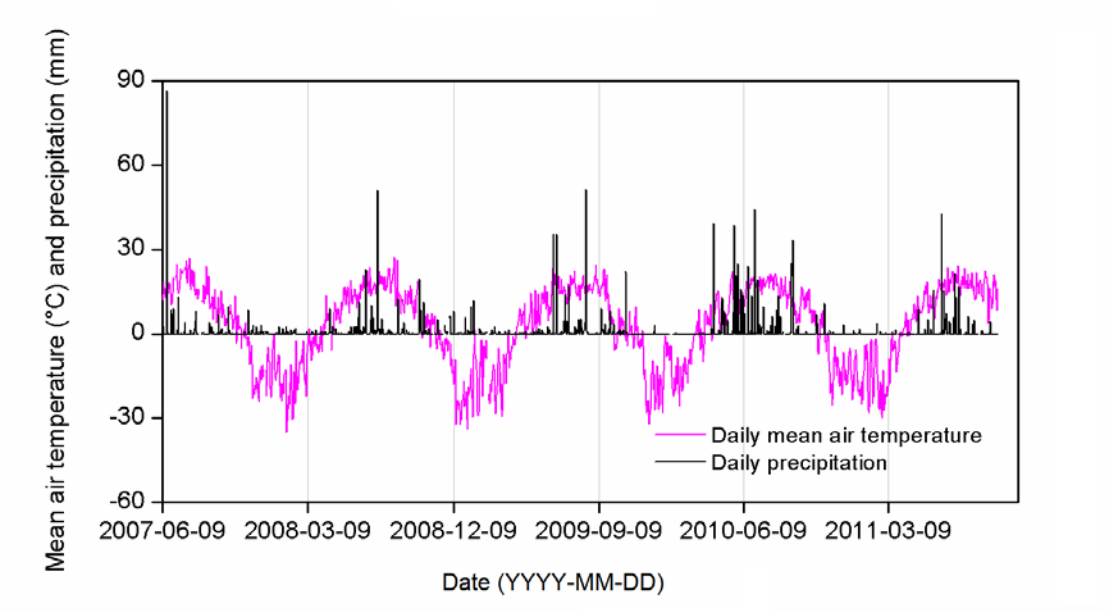

Fig. 2. Daily mean air temperature and precipitation during the study period.

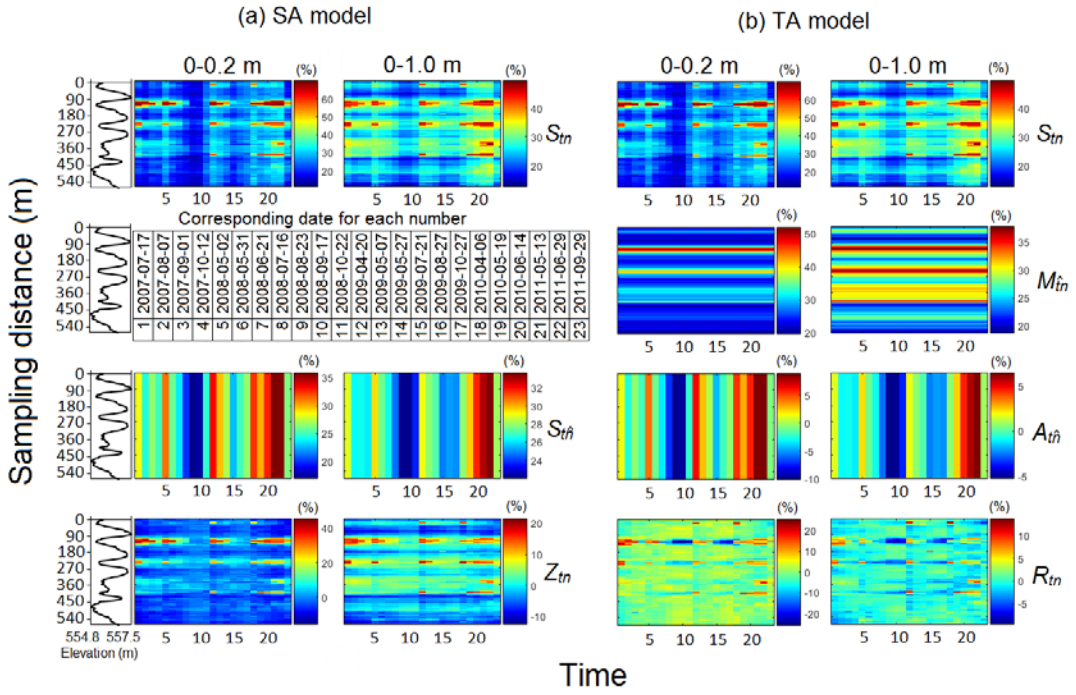

Fig. 3. Components of soil water content in (a) the SA model (spatial mean soil water content $S_{t\hat{n}}$ and spatial anomaly Z_{tn}) and in (b) the TA model (time-stable pattern $M_{\hat{t}n}$, space-invariant temporal anomaly $A_{t\hat{n}}$, and space-variant temporal anomaly R_{tn}) for 0–0.2 and 0–1.0 m. Also shown is the elevation.

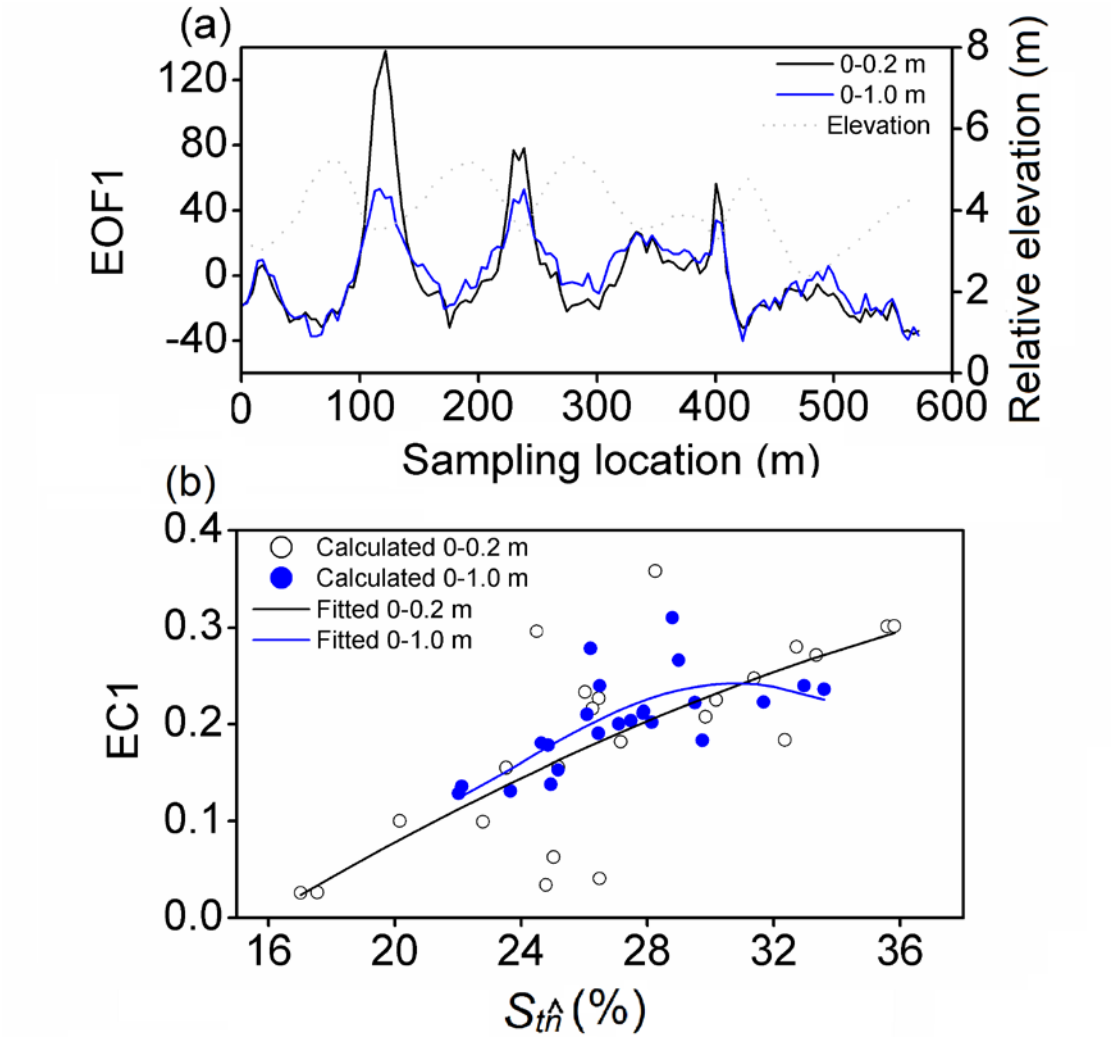

Fig. 4. (a) The EOF1 of the spatial anomaly Z_{tn} and (b) relationships of associated EC1 versus spatial mean soil water content Z_{tn} fitted by the cosine function (Eq. 4).

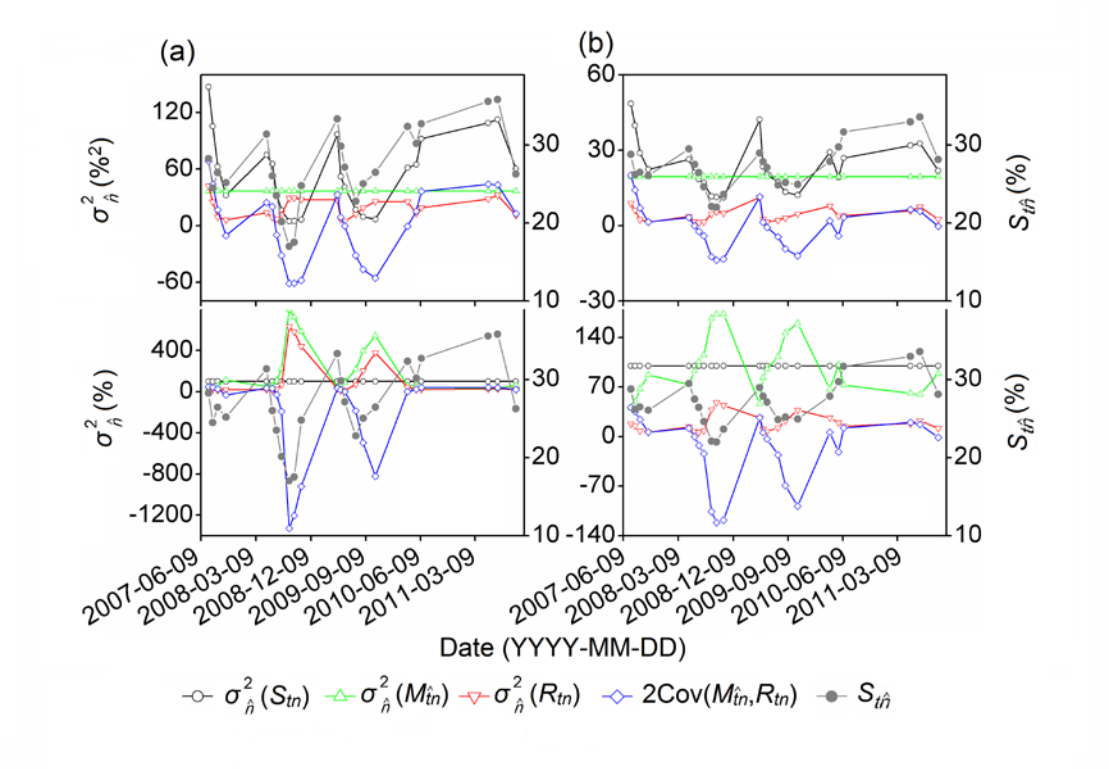

Fig. 5. Spatial variances of different components in Eq. (8) expressed in $\%^2$ (upper panel) and as percentage (lower panel) for (a) 0–0.2 and (b) 0–1.0 m. Spatial mean soil water content $S_{t\hat{n}}$ on each measurement day is also shown.

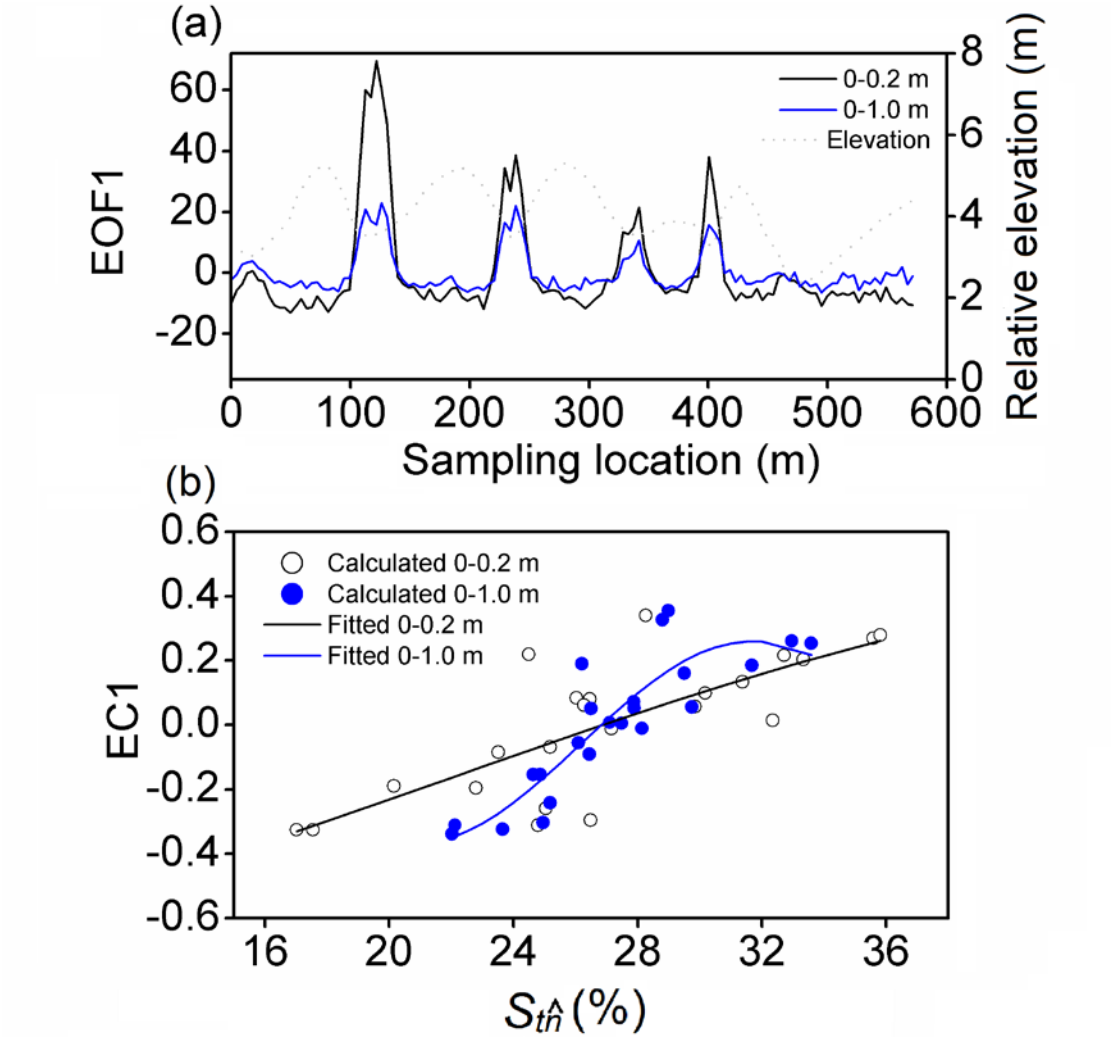

Fig. 6. (a) The EOF1 of the space-variant temporal anomaly R_{tn} and (b) relationships of associated EC1 versus spatial mean soil water content $S_{t\hat{n}}$ fitted by the cosine function (Eq. 4).

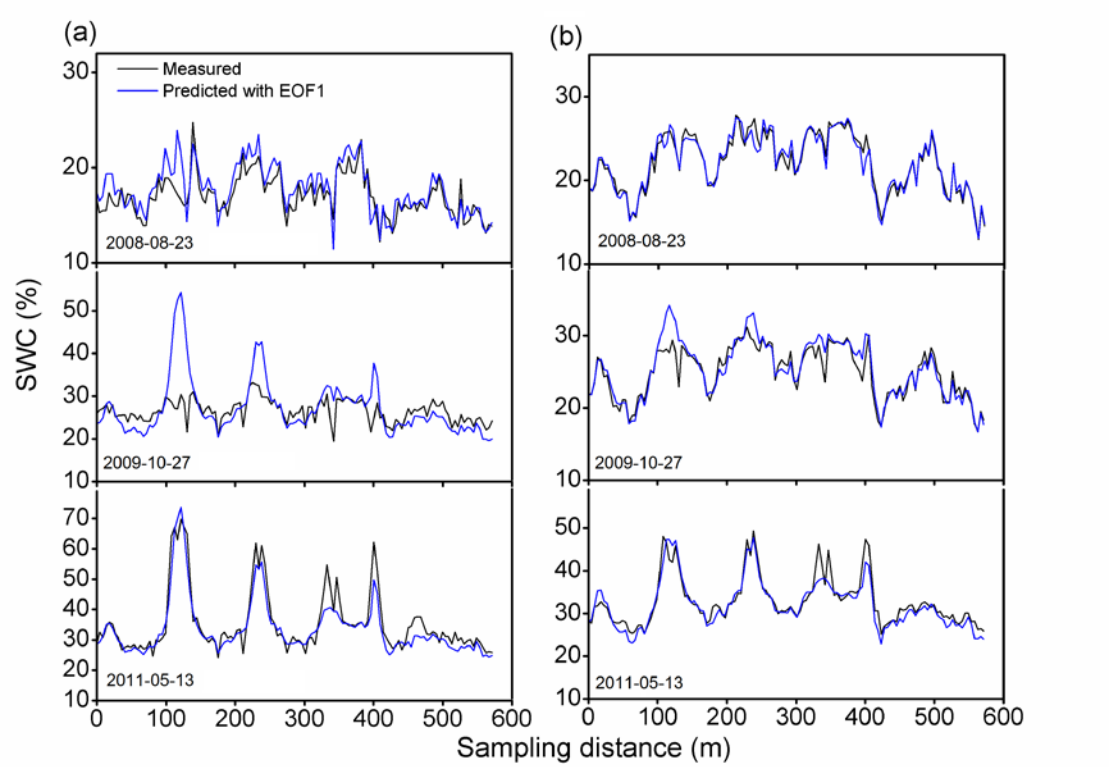

Fig. 7. Estimated soil water content (SWC) versus measured SWC for three dates at different soil water conditions (August 23, 2008, October 27, 2009, and May 13, 2011 are associated with relatively dry, medium, and wet days, respectively) using the TA model for (a) 0–0.2 and (b) 0–1.0 m.

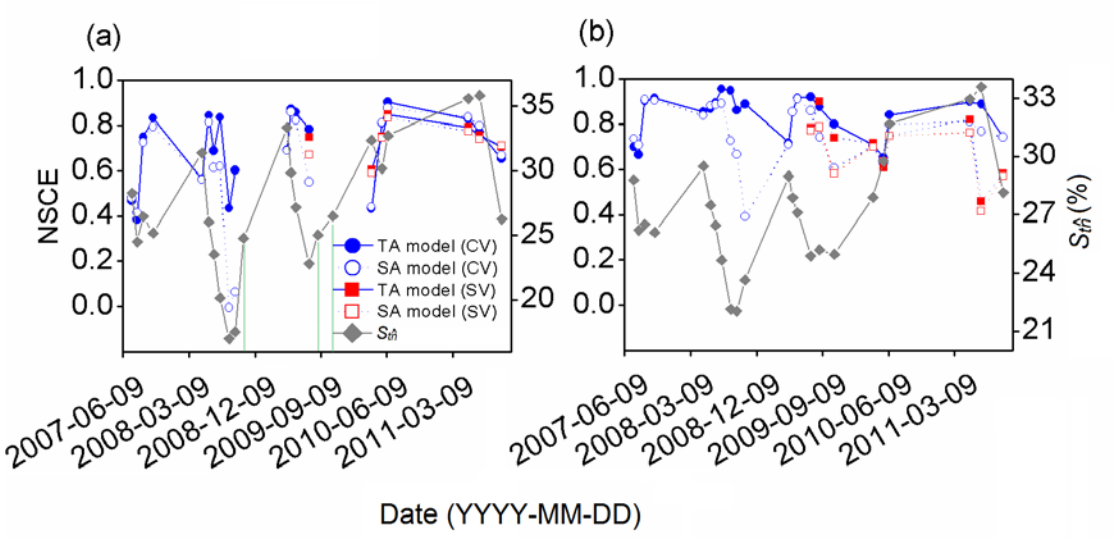

Fig. 8. The Nash-Sutcliffe coefficient of efficiency (NSCE) of soil water content estimation using the TA and SA models for (a) 0–0.2 and (b) 0–1.0 m for both cross validation (CV) and split sample validation (SV). At 0–0.2 m, three dates (October 22, 2008, August 27, 2009, and October 27, 2009) as indicated by green lines present negative NSCE values (-4.05, -1.83, and -3.81, respectively, for the CV on the three dates; -2.63 and -5.12, respectively, for the SV on the latter two dates). Spatial mean soil water content $S_{t\hat{n}}$ on each measurement day is also shown.

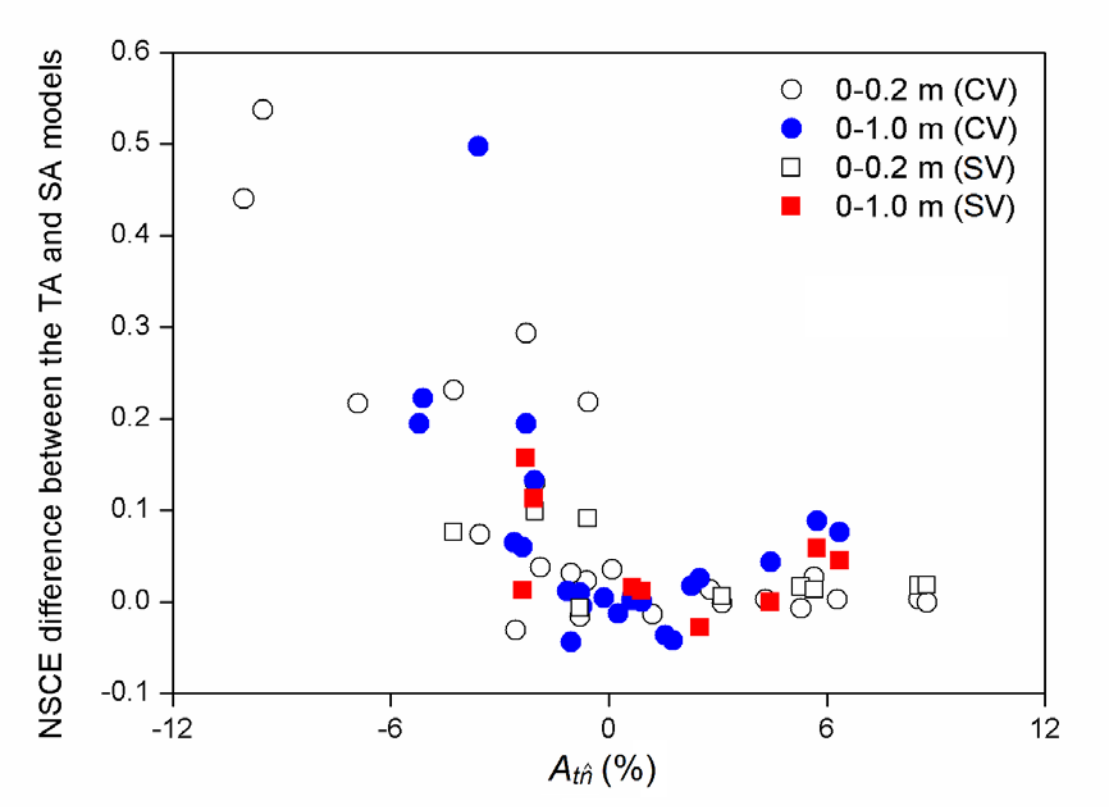

Fig. 9. Nash-Sutcliffe coefficient of efficiency (NSCE) difference between the TA and SA models in terms of soil water content estimation using both cross validation (CV) and split sample validation (SV) as a function of space-invariant temporal anomaly $A_{t\hat{n}}$ for (a) 0–0.2 and (b) 0–1.0 m.

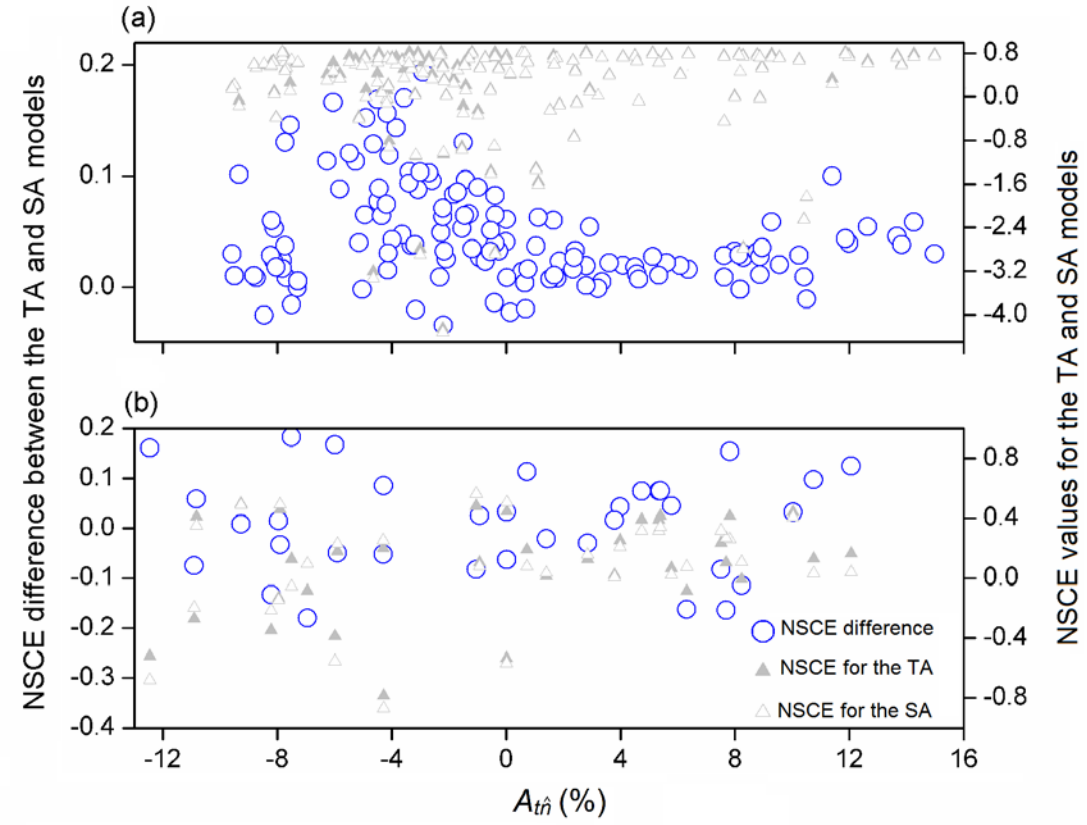

Fig. 10. Nash-Sutcliffe coefficient of efficiency (NSCE) difference between the TA and SA models in terms of soil water content estimation using cross validation as a function of space-invariant temporal anomaly $A_{t\hat{n}}$ for (a) 0–0.06 m of the Chinese Loess Plateau hillslope and (b) 0–0.15 m of the GENCAI network in Italy. The NSCE values for both models are also shown.